




Heteronuclear multicolor soliton compounds induced by convex-concave phase in fiber lasers

Heze Zhang¹, Dong Mao¹  [✉], Yueqing Du¹, Chao Zeng¹, Zhipei Sun²  & Jianlin Zhao¹ 

Optical solitons emerging from fiber resonators generally possess similar properties that hinge on the system parameters. However, the generation of wavepackets composed of dissimilar solitons within the same laser cavity is still challenging in ultrafast lasers. Here, we report on heteronuclear multicolor soliton compounds composed of chirp-free conventional solitons and chirped dissipative solitons, by introducing convex-concave frequency phases in mode-locked fiber lasers. In spite of different lasing wavelengths, the dissipative solitons always overlap with the conventional solitons, giving birth to trains of modulated wavepackets. The resonant sidebands of two types of solitons follow from the same phase-matching principle dominated by the absolute value of cavity dispersion. Simulations fully substantiate the experimental results, confirming that the overlapping of two solitons is dominated by the co-action of saturable absorption and group-delay compensation. It is demonstrated that the phase-managed dissipative system is capable of supporting multicolor soliton compounds with distinct properties, offering an effective platform to reveal the interaction of dissimilar nonlinear wavepackets.

¹MOE Key Laboratory of Material Physics and Chemistry Under Extraordinary Conditions, and Key Laboratory of Light Field Manipulation and Information Acquisition, Ministry of Industry and Information Technology, School of Physical Science and Technology, Northwestern Polytechnical University, Xi'an 710129, China. ²Department of Electronics and Nanoengineering and QTF Centre of Excellence, Aalto University, Aalto, Finland. ✉email: maodong@nwpu.edu.cn

Soliton is a self-organized wavepacket that preserves its shape during propagation in the dispersive-nonlinear medium, which is a ubiquitous phenomenon in nature and has been widely studied in various fields, ranging from hydrodynamics¹, Bose–Einstein condensates², event astronomy³ to biomedicines⁴. In the category of nonlinear optics, a chirp-free soliton that propagates in a particle-like fashion can be formed ascribing to the delicate balance between nonlinearity and anomalous dispersion of fibers or fiber lasers⁵. Via engineering the dispersion to near-zero and normal regime, stretched pulses⁶, similaritons⁷ and dissipative solitons (DSs)^{8,9} have been realized in fiber lasers under the complex interaction among dispersion, nonlinearity, gain and loss. Broadly speaking, the aforementioned pulses in fiber laser can be categorized as DSs since they are formed in non-conservative dissipative systems balanced by energy exchange with the external environment in the presence of fiber dispersion and nonlinearity. In a narrow sense, DSs here refer to confined wavepackets of light formed in normal dispersion regimes, in which the pulse experiences strong nonlinear gain and loss during propagation and usually features a giant frequency chirp⁸. Due to the gain competition effect, fiber lasers usually operate at the single-wavelength emission state, delivering a fixed type of robust pulse that depends on cavity parameters. By introducing spectral filters into the cavity, multicolor operations were realized at 1.06 μm , 1.55 μm , and 2 μm in mode-locked fiber lasers^{10–14}. Attributing to the chromatic dispersion, the group velocities of these multicolor pulses differ from each other, resulting in independently evolved multiple pulse trains¹².

Meanwhile, synchronization and overlap of pulses at different wavelengths give birth to multicolor wavepackets with fine temporal structures due to the beat effect, which is especially attractive for coherent combining, terahertz-wave generation, and Raman scattering spectroscopy^{15–17}. Several active and passive methods have been proposed for synchronizing two-branch pulses at different wavelengths, such as phase-locked loop¹⁸, balanced optical cross-correlator¹⁹, and slave–master cavity configuration²⁰. With the help of the filtering effect, fiber laser could directly deliver synchronized dual-color solitons via tailoring the cavity dispersion to near-zero regime^{21,22}, or compensating the group-velocity mismatch by intermodal dispersion²³. Apart from these approaches, the stimulated Raman scattering is proven to be able to generate multicolor bound chirped DS in fiber lasers²⁴.

Recently, active manipulation of cavity parameters has advanced the development of solitons to an unprecedented state^{25–27}. Runge et al. achieved high-energy pure-quartic solitons in fiber laser via introducing fourth-order dispersion and eliminating the second- and third-order dispersion of cavity²⁸. After that, synchronized multicolor solitons²⁹ and spectrally periodic pulses³⁰, as the newly emerged nonlinear wavepackets, were achieved by engineering the dispersion of fiber laser with a programmable pulse shaper. These synchronized multicolor pulses are generated at the same dispersion regime, whose constituent pulses exhibit similar properties. Lately, dark-bright dual-color soliton pairs and broadband microcombs operating in opposite dispersion regimes were achieved in a micro-resonator under the effect of cross-phase modulation^{31,32}. However, the dispersion characteristic of such a resonator cannot be actively manipulated. It is still unclear whether fiber lasers could support special wavepackets composed of dissimilar solitons, i.e., heteronuclear multicolor soliton compounds (HMSCs). Moreover, the interaction between distinct types of solitons remains less addressed in nonlinear dissipative systems.

In this paper, we demonstrate HMSCs in a mode-locked fiber laser, by introducing convex–concave phase and spectral filtering with a programmable pulse shaper. The convex–concave phase

grants the periodic anomalous-normal dispersion distribution in the frequency domain, enabling the formation of the chirp-free conventional soliton (CS) and chirped DS in the same fiber laser. Different from the previous reports demonstrating the coexistence of two types of pulses with different group velocities^{13,33}, the CS and DS with distinct wavelengths always co-propagate as a unit with fine temporal structure, forming a robust multicolor soliton compound composed of dissimilar solitons. Moreover, the DS here displays unique sidebands that can be controlled by the frequency phase, whose formation is not attributed to the nonlinear phase shift, but follows from the similar phase-matching principle as that of CS. Simulations validate the crucial experimental phenomena and reveal the interaction behavior between two distinct types of solitons.

Results

Experimental setup and results. Figure 1a shows the cavity configuration of the HMSC fiber laser. The 980-nm laser diode pumps a 6-m erbium-doped fiber (Nufern: EDFL-980-HP, $\beta_2 = 21.3 \text{ ps}^2 \text{ km}^{-1}$) via a wavelength-division multiplexer, and the optical coupler extracts 10% energy for measurement. A polarization-insensitive isolator ensures the unidirectional propagation of pulses, and a programmable pulse shaper introduces the convex–concave phase and spectral filtering. The carbon nanotube saturable absorber initializes the mode-locking operation of the laser. The pigtailed fiber components are standard single-mode fibers (Corning: SMF-28e+, $\beta_2 = -21.7 \text{ ps}^2 \text{ km}^{-1}$) with a total length of 9.2 m, and the programmable pulse shaper has an optical path of 3.7 m with an intrinsic dispersion of -0.45 ps^2 . Based on the above parameters, the total length and cavity dispersion are 18.9 m and -0.52 ps^2 , respectively.

The programmable pulse shaper (Santec, WSS-1000), composed of a diffraction grating and spatial light modulator, can arbitrarily adjust the amplitude and phase of each spectral component through a computer, and its principle is depicted in the left panel of Fig. 1b. Based on the Taylor series expansion of spectral phase³⁴, the parabolic convex–concave frequency phase corresponds to a linear group delay with opposite slopes and an anomalous-normal dispersion regime (right panel of Fig. 1b). Therefore, the opposite dispersion regimes can be achieved within the same laser resonator by introducing the convex–concave phase, enabling the formation of HMSC composed of dissimilar solitons.

For each waveband, the dispersion depends not only on the cavity parameters, but also on the frequency phase induced by the programmable pulse shaper. As shown in Fig. 2a, after introducing the convex–concave phase, the group-delay dispersions at shorter and longer wavebands are about -15.38 ps^2 and 14.33 ps^2 , respectively. Hence, the convex phase (i.e., shorter waveband) corresponds to the anomalous-dispersion regime, enabling the formation of CS characterized by Kelly sidebands³⁵ and Sech² spectral profile that is somewhat similar to the convex phase. The longer waveband locates at the normal dispersion regime, where the spectrum mimics the concave phase with a low-intensity center and strong sidebands, referred to as the DS. Note that the amplitudes of the convex–concave phase are the relative values, the phase jump (red curve in Fig. 2a) does not influence the values of group-delay dispersion at two wavebands.

Decreasing the amplitude of concave phase while keeping the convex phase unchanged, the spectrum of mode-locked pulse at longer waveband is gradually close to the typical DS observed in normal dispersion lasers. For example, the DS in Fig. 2b exhibits a “cat-ear” structure that is similar to the spectral profiles of the previously reported DSs³⁶. In contrast to the spectral peaks arising from the nonlinear phase shift³⁷, the “cat-ear” structure

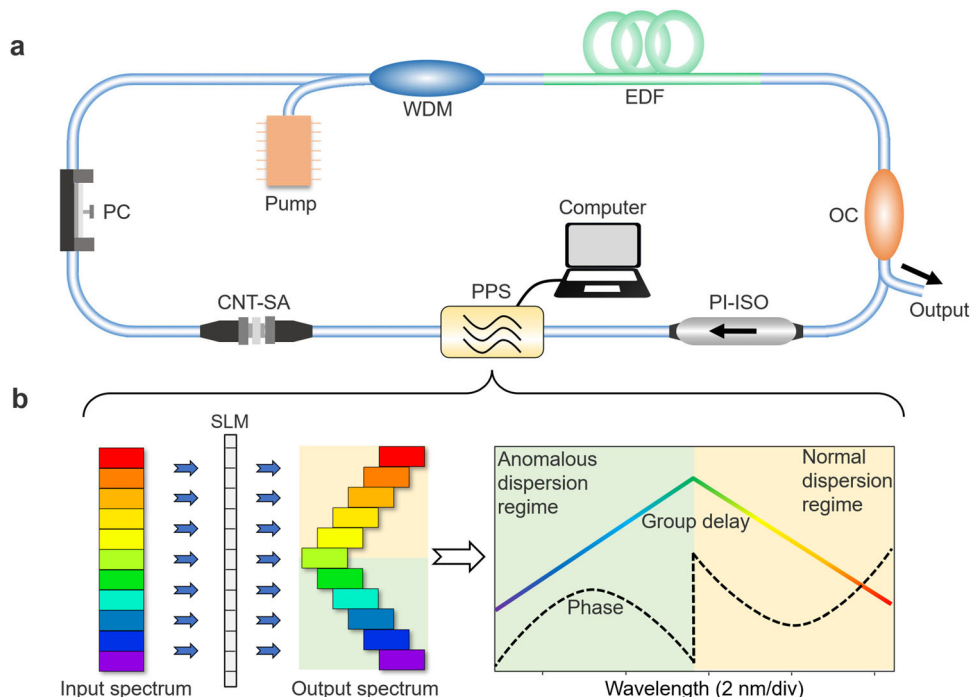


Fig. 1 Heteronuclear multicolor soliton compound (HMSC) fiber laser. **a** Experimental setup. WDM wavelength division multiplexer; EDF erbium-doped fiber; OC output coupler; PI-SO polarization-insensitive isolator; PPS programmable pulse shaper; PC polarization controller; CNT-SA carbon nanotube saturable absorber. **b** Principle and function of PPS. The black dashed curve denotes the convex-concave frequency phase, which corresponds to a linear group delay with opposite slopes and an anomalous-normal dispersion regime.

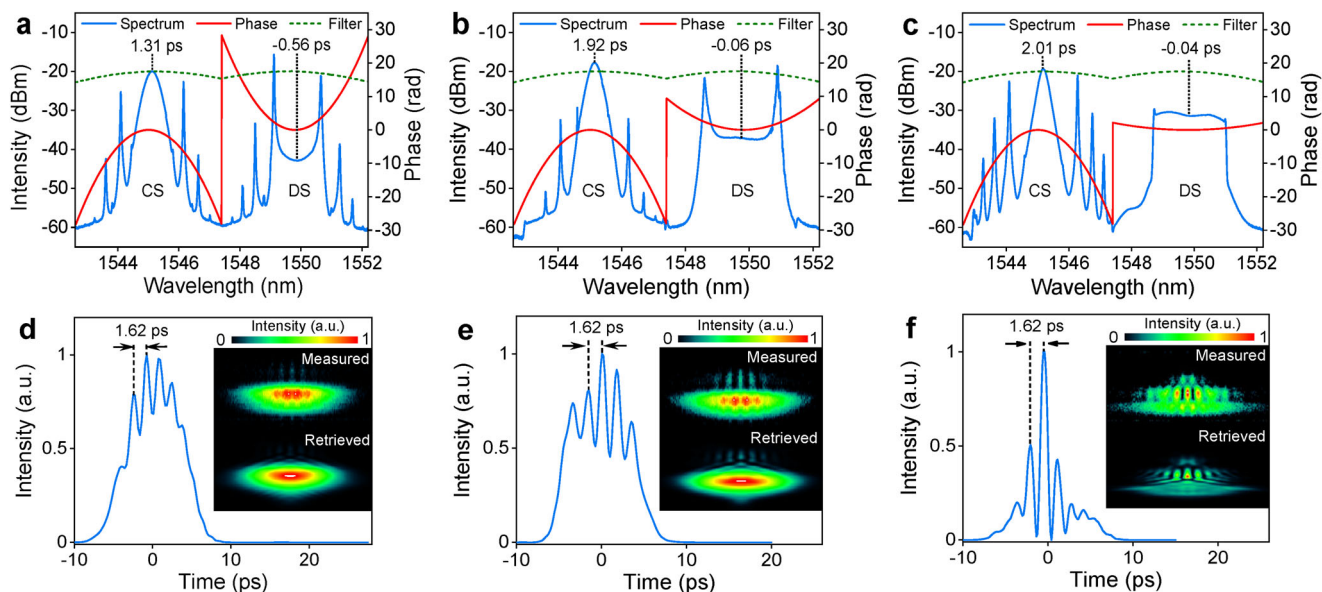


Fig. 2 Properties of HMSC with different amplitudes of concave phase. CS conventional soliton. DS dissipative soliton. **a-c** Spectra, phases, and filtering. **d-f** Retrieved pulses and frequency-resolved optical gating spectrograms.

here belongs to the first-order dispersive sideband of DS, which will be elaborated in the next part. The DS exhibits the characteristic quasi-rectangular spectrum and possesses comparable intensity with CS when further decreasing the amplitude of concave phase (Fig. 2c). Note that the pulse profiles retrieved from the frequency-resolved optical gating spectrograms show beat fringes with the same period of 1.62 ps (Fig. 2d–f), coinciding with the central wavelength separation of 4.76 nm between CS and DS according to the Fourier transform principle. The beat fringe validates the overlapping of two solitons, which is further

corroborated by the radio-frequency spectrum and oscilloscope trace (see details in Supplementary Note 1).

The properties of CS and DS are further revealed by spectrally filtering the HMSC external to the cavity (see Supplementary Note 2). The time-bandwidth products of the CS and DS are given as 0.32 and 0.95, respectively, which confirms that the CS is chirp-free while the DS is chirped. The separations of beat fringe for three cases are identical (1.62 ps) due to the constant wavelength spacing between two solitons. Note that the group-delay differences between two spectral centers induced by

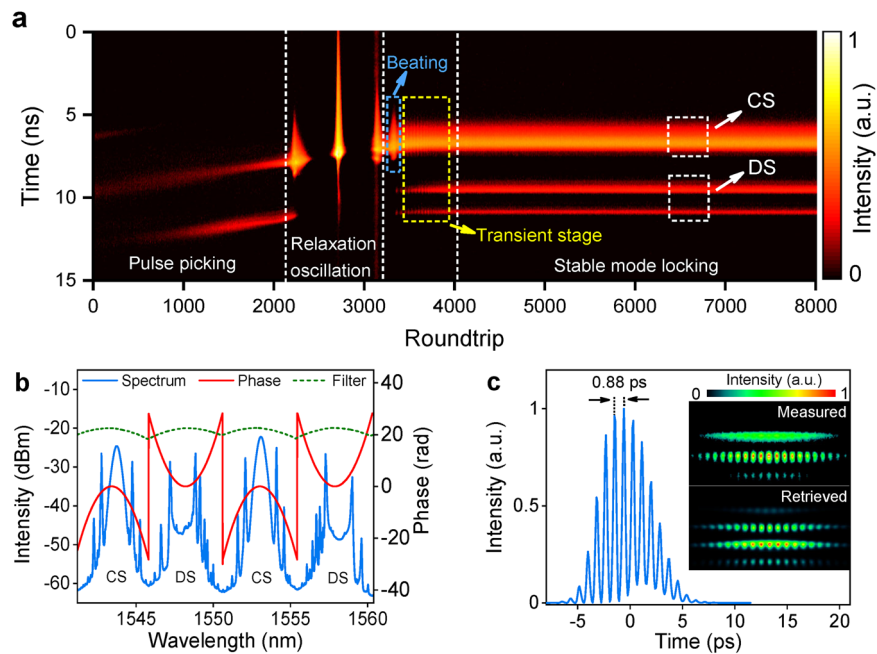


Fig. 3 Build-up process of dual-color HMSC and properties of four-color HMSC. CS conventional soliton. DS dissipative soliton. **a** Real-time spectrum evolution. **b, c** Spectrum, phase, filtering, retrieved pulse, and frequency-resolved optical gating spectrograms of four-color HMSC.

convex–concave phases are 1.87 ps, 1.98 ps, and 2.06 ps, respectively, which nearly compensate for the intrinsic group-delay difference of fiber laser (-1.94 ps). In spite of the small residual group-delay differences, the saturable absorber automatically forces two solitons into a trapped state as the overlapped pulse has a higher intensity and thus results in a lower non-saturable loss. It is demonstrated that the HMSC fiber laser also follows from the same minimum-loss principle reported on the spatiotemporal mode-locked laser³⁸.

By exploiting time-stretch dispersive Fourier transform technique^{39–42}, we record the build-up process of the HMSC in Fig. 2a. The details of the measurement system are given in the “Methods” section. As depicted in Fig. 3a, the lasing wave undergoes a pulse-picking process from 0 to ~ 2100 roundtrips, wherein the weak noisy pulses are eliminated by the saturable absorber and the dominant pulses survive. Then, the laser enters the relaxation oscillation stage, lasting ~ 1000 roundtrips (from 2100 to 3100 roundtrips). After the beating stage, the metastable CS and DS appear at ~ 3200 roundtrips and experience a transient stage with damped breathing behavior. The fiber laser finally evolves into the steady state at ~ 4000 roundtrips, forming the stable dual-color HMSC. The build-up process is somewhat similar to previously reported fiber laser⁴³, while the lasting time is much longer than that of CS⁴⁴ or CS compounds²⁹, which is attributed to the harsher formation condition of HMSCs. At the steady state, only CS and first-order sidebands of DS are captured as their other spectral components are relatively weak. One can find that the CS and DS reach the steady state at the same time, and they always synchronously circulate inside the cavity.

In addition to dual-color HMSCs, three- to five-color HMSCs can also be achieved in the same fiber laser by increasing the filter bandwidth from 14.4 nm to 19.1 nm and introducing more concave and convex phases into the cavity (see details in Supplementary Note 3). Figure 3b shows the typical case of four-color HMSC comprising two CSs and two DSs. The retrieved pulse exhibits a clear beat fringe (Fig. 3c), which is attributed to the overlap of these solitons. Note that the beat fringe separation (0.88 ps) corresponds to the wavelength separation between two CSs (9.38 nm). This is because, the

intensity of DS is much lower than CS, and the beat fringe is dominated by two CSs. The synchronization of these solitons can be further corroborated by the oscilloscope trace and radio-frequency spectrum (see Supplementary Note 1).

Formation mechanism of sideband on DS. When pulses encounter periodic perturbations such as gain, filtering effect and loss in a fiber laser, they shed parts of energy in the form of dispersive waves⁴⁵. The dispersive waves generated at the adjacent roundtrip interfere, and only the frequencies satisfying the phase-matching principle survive in the cavity. Figure 4a, b shows the phase-matching conditions of the dispersive wave for CS and DS, respectively. The blue horizontal line and curve denote the phases of CS (φ_{CS}) and DS (φ_{DS}) accumulated per roundtrip, respectively. The parabolic lines are phases of dispersive waves (φ_{DW}) accumulated in one roundtrip:

$$\varphi_{DW} = \frac{1}{2}\beta_2(\delta f \times 2\pi)^2 L \quad (1)$$

where β_2 is the group-velocity dispersion of the fiber laser, δf is the frequency offset from the spectral center, and L is the cavity length. As the introduced convex (concave) phase spans from $-\pi$ to 0 ($0-9\pi$) in the studied waveband, the phase-matching between dispersive wave and pulse is achieved at several frequencies when the phase difference is the integer multiple of 2π . Note that no particular periodic perturbation is required for the first-order phase-matched frequency of DS (red dot in Fig. 4b), as the accumulated phase shift always matches that of the dispersive waves at any cavity position⁴⁶. This condition is unpractical for CS unless the laser cavity has strong third-order dispersion⁴⁷.

Based on the phase-matching principle between the dispersive waves and solitons⁴⁸, the relationship between two adjacent sidebands on one side can be expressed as:

$$(\delta f_m)^2 - (\delta f_{m-1})^2 = \frac{1}{\pi|\beta_2|L}, \quad (2)$$

where δf_m and δf_{m-1} are frequency offsets between the spectral center and sidebands with the order of m and $m-1$ ($m \geq 2$), respectively.

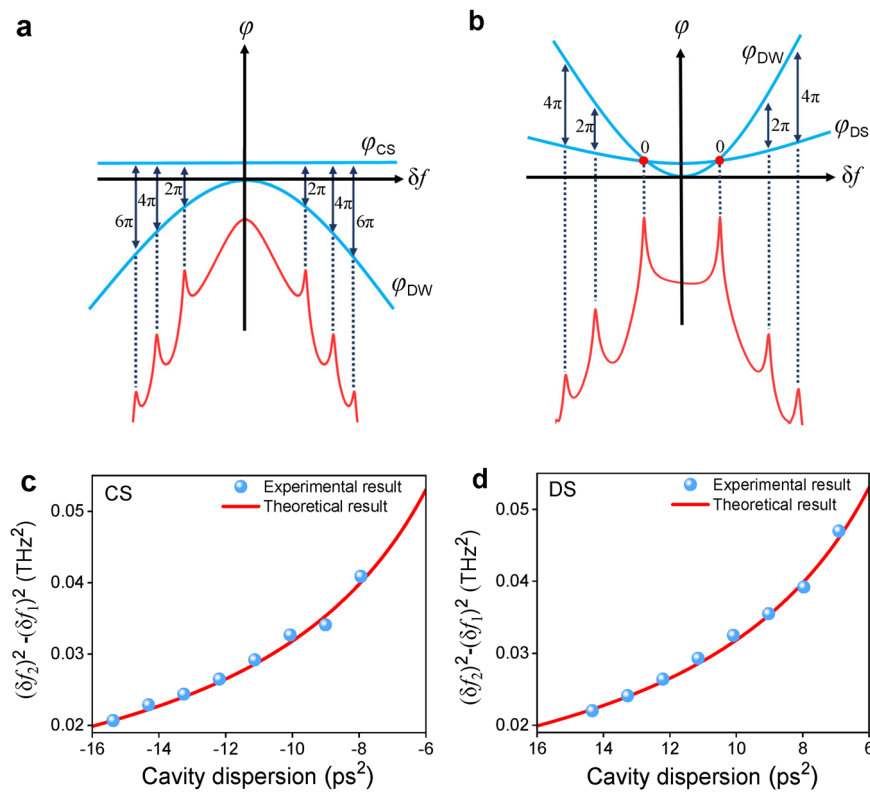


Fig. 4 Spectral sidebands arising from the phase-matching principle. CS conventional soliton. DS dissipative soliton. **a, b** The phase φ versus frequency offset δf for CS and DS, respectively. **c, d** Squared difference of frequency offsets between first- and second-order sidebands versus cavity dispersion. The experimental points (blue dots) are calculated from the measured spectra, their slight deviations from theoretical results are mainly attributed to the accuracy of the optical spectrum analyzer.

Via changing the amplitude of concave and convex phases (i.e., changing group-velocity dispersions at two wavebands), we calculate the squared difference of frequency offsets between first- and second-order sidebands for CS and DS based on Eq. (2), respectively. As illustrated in Fig. 4c, d, the theoretical prediction agrees with experimental observation, verifying that the strong sidebands of DS arise from the resonant amplification of dispersive waves rather than the nonlinear phase shift accumulated in the cavity. It turns out that the sidebands of CS and DS follow the same phase-matching principle that mainly depends on the absolute value of cavity dispersion.

Simulation results. To uncover the formation mechanism of HMSCs, we perform numerical simulation based on the generalized nonlinear Schrödinger equation that incorporates nonlinearity, dispersion, gain and loss of fiber resonator^{29,41}. The simulation starts from a weak noisy pulse, and the pulse enters the loop and passes through each fiber component sequentially. After one circulation, the resultant pulse works as the input of the next roundtrip until the fiber laser achieves a self-consistent state (see details in “Methods”).

Figure 5 shows the simulation results of three typical HMSCs, which agree well with the experimental counterparts, from spectral profiles to evolution behaviors. The separation between two spectral centers is 5.02 nm, also comparable with the experimental result of 4.76 nm (Fig. 5a–c). In the simulation, the group-delay differences induced by the convex–concave phase almost compensate for the intrinsic group-delay difference of the cavity. Although two solitons have different wavelengths, they always overlap and evolve as a unit in the cavity (Fig. 5d–f), verified by the temporal beat fringes (Fig. 5g–i). The insets of Fig. 5g–i show that the DS accumulates a linear frequency chirp,

which is the typical characteristic of mode-locked pulse in normal dispersion lasers. In addition, the spectrograms show that the sidebands of CS on the blue (red) side locate at the pulse leading (trailing) edge, while it is opposite for DS, confirming that two constituents of HMSCs operate at opposite dispersion regimes.

Reducing the amplitude of the concave phase, the energy of DS transfers from the sideband to the central region of the spectrum, which also can be interpreted by the phase-matching principle. As depicted in Fig. 4b, the central frequency of DS deviates from the phase-matching condition. Such deviation becomes less apparent for the smaller amplitude of the concave phase, and the central frequency is capable of receiving more energy, leading to the energy transformation within the DS. Correspondingly, the pulse intensity increases while the duration decreases during this evolution. For previously reported DS fiber lasers⁴⁹, the cavity dispersions are usually less than 2ps^2 , which is much smaller than the cases of Figs. 2a and 5a. Thus, the phase-matching effect is less important, and the sidebands disappear on the spectrum.

Note that the CS can always be formed in the fiber laser with or without the convex phase. However, the DS is unable to exist alone and always accompanies the CS, i.e., the CS and DS with distinct properties appear as a unit. Such a phenomenon is understandable by noting that DS requires a harsher formation condition than CS. For example, considering the self-phase modulation effect, the DS will be quickly broadened by normal dispersion while the CS may survive in the presence of anomalous dispersion. Notably, the DS has a much lower intensity than that of CS. As the transmittance of the saturable absorber relies on the pulse intensity, the DS will be eliminated due to the saturable absorption effect while the CS could survive due to the higher pulse intensity.

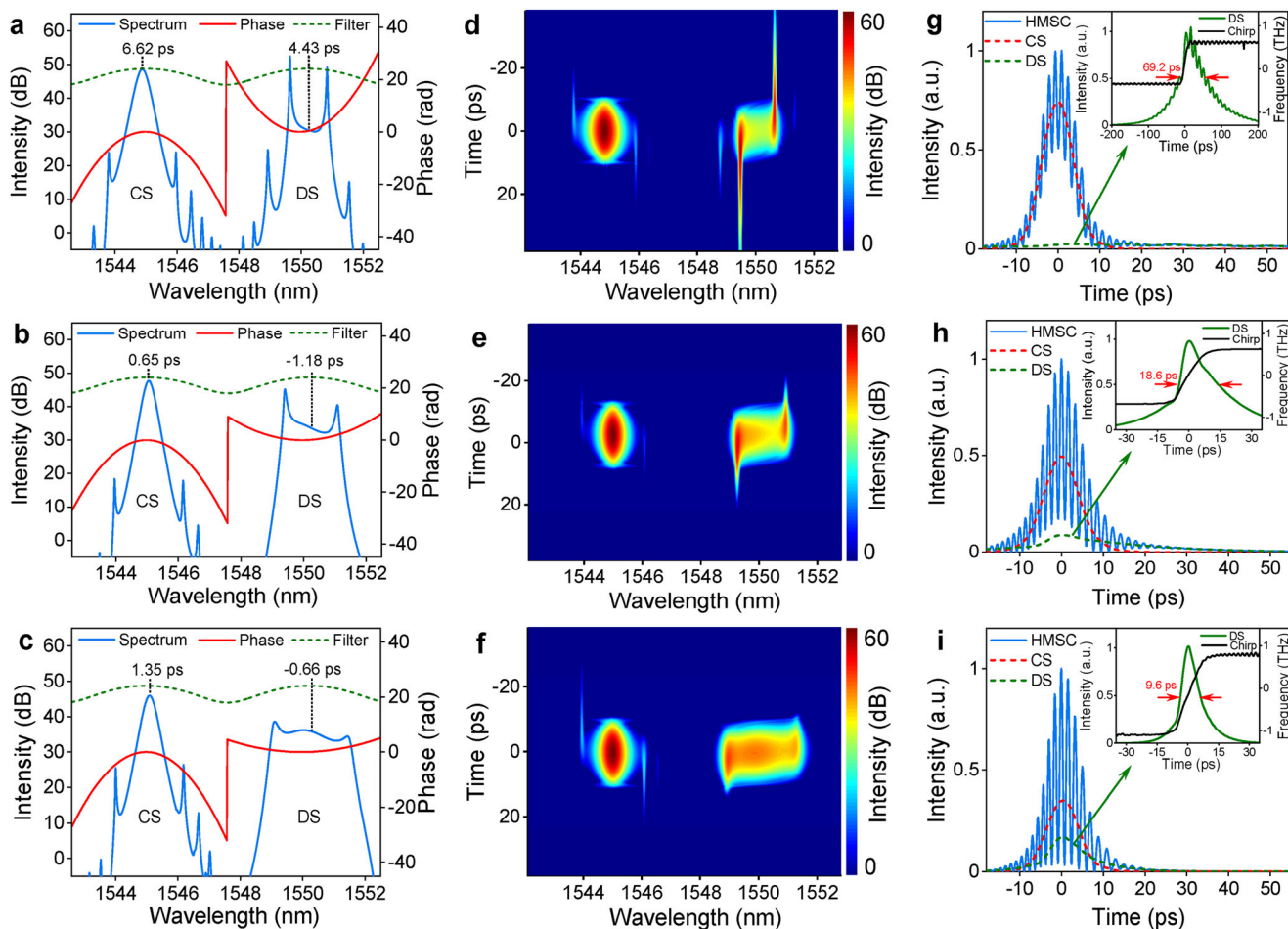


Fig. 5 Simulation results of HMSC for different concave phases. CS conventional soliton. DS dissipative soliton. **a-c** Spectra, phases and filtering. **d-f** Spectrograms. **g-i** Profiles of HMSC, CS and DS. The insets show frequency chirps and profiles of DS.

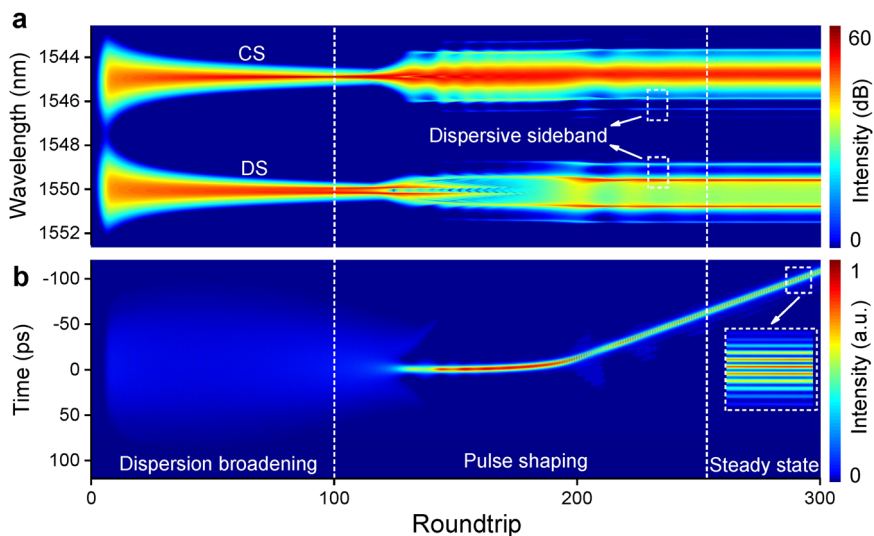


Fig. 6 Simulated build-up process of HMSC. CS conventional soliton. DS dissipative soliton. **a, b** Spectrum and pulse evolutions versus roundtrip number. The CS and DS are overlapped during the whole build-up process, and reach the steady state at the same time, similar to the experimental observations.

We further simulate the build-up process of HMSC in Fig. 5a to reveal the underlying mechanism, as shown in Fig. 6. The initial noisy pulses quickly broaden, and the spectral widths of CS and DS gradually decrease from 0 to 100 roundtrips, wherein the dispersion dominates this process. Then, the pulse envelope starts

to narrow and new spectral components emerge under the effect of self-phase modulation and saturable absorption effects. In this stage, the spectrum of DS splits into two parts while that of CS maintains the Sech^2 profile, which is attributed to the opposite dispersion settings at two wavebands. After that, the dispersive

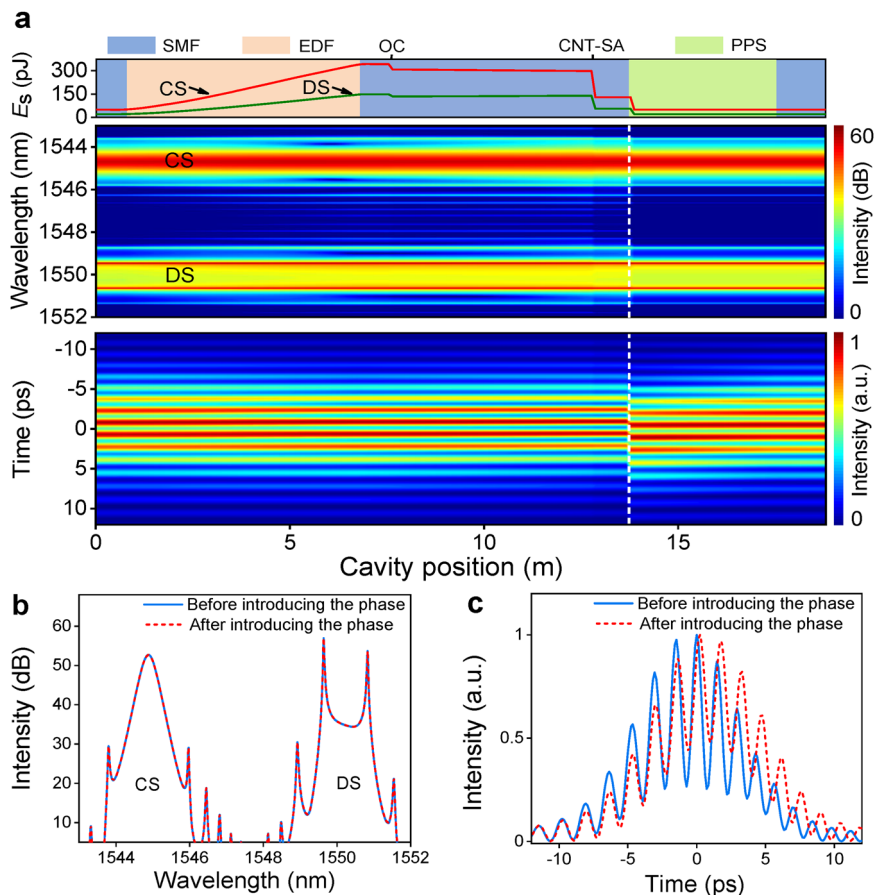


Fig. 7 Intracavity evolution of HMSC. CS conventional soliton. DS dissipative soliton. **a** Energy, spectrum, and pulse evolutions versus cavity position. The white dashed line denotes the position where we impart the phase into the cavity. **b, c** Spectra and pulse profiles before and after introducing the phase.

sidebands gradually formed on the spectra of CS and DS under the phase-matching effect, reaching a metastable state at ~ 150 roundtrips. Finally, the pulse evolves to a steady state after a complex pulse-shaping process. Since the CS contains most of the energy of the HMSC and the reference wavelength is 1548 nm, the pulse shifts toward the forefront of the time window. Note that two solitons reach the steady state at the same time, coinciding with the experimental observation in Fig. 3a.

During the whole build-up process, two solitons always overlap in the time domain, giving rise to the HMSC with periodic structures. This can be attributed to the co-action of saturable absorption and the group-delay compensation. To verify this, we further simulate the HMSC evolution with respect to cavity roundtrips in the absence of the saturable absorber or convex-concave phase (i.e., group-delay compensation), respectively (see details in Supplementary Note 4). When the saturable absorber is removed in the simulation model, two pulses still overlap under the group-delay compensation, whereas they broaden due to the chromatic dispersion and strongly emit non-solitary radiation per roundtrip. Once the group-delay compensation is ignored, two solitons propagate at different velocities and quickly depart from each other under the effect of chromatic dispersion.

The intracavity evolution of HMSC in a single roundtrip is shown in Fig. 7. For simplicity, the HMSC in Fig. 5a is discussed, while the other cases are given in Supplementary Note 5. The intracavity energy evolutions of CS and DS are shown in the upper panel of Fig. 7a. Due to the filtering effect, the spectral width of DS is less than 3 nm, thus the corresponding energy is significantly confined, resulting in comparable energy with CS.

Moreover, the CS makes the saturable absorber easier to saturate, and thus the DS can be formed at a relatively low intensity. In the cavity, two solitons are amplified in the erbium-doped fiber segment and then weakened by the single-mode fiber, output coupler, saturable absorber, and programmable pulse shaper to realize a self-consistent evolution. The intensities of spectrum and pulse are normalized at each cavity position to highlight the imperceptible changes of the wavepacket. As shown in the middle and lower panels of Fig. 7a, the spectral profiles of CS and DS nearly keep invariant along the cavity, which results from the limited pulse intensity. Ascribing to the fixed wavelength separation between two solitons, the beat fringe of HMSC almost remains unaltered along the cavity. The white dashed line denotes the position of the introduced phase. One can observe that, the phase does not influence the spectral intensity (Fig. 7b), while affecting the temporal properties, i.e., weakens the modulation depth and changes the pulse location (Fig. 7c). Note that the first-order sidebands (or cat-ear structure) of DS always appear at the same frequency inside the cavity. In contrast, such “cat-ear” structure on previously reported DS arises from the nonlinear phase shift, periodically emerging and disappearing within the cavity due to the spectral filtering effect³⁶. Since the “cat-ear” structure induced by nonlinear phase shift changes along the cavity, we further confirm that the sidebands of DS in our experiment arise from the phase-matching effect.

Conclusion

It is apparent that the resonant radiation from the soliton is a universal phenomenon independent of the dispersion regime. The difference is that, the central frequency is phase-matched for

CS while phase-mismatched for DS. The synchronization between CS and DS is mainly attributed to the group-delay compensation, then the saturable absorption effect forces them to overlap to minimize the transmission loss, following from the principle of minimum loss in mode-locked lasers³⁸. Besides, the filtering effect is also essential in the formation of HMSCs, which is verified by the pulse evolution in the cavity without the spectral filtering (see Supplementary Note 6). One can find that the HMSC cannot be maintained and quickly collapses into multiple sub-pulses after 10 roundtrips. Thus, the formation of such wavepackets relies on three key factors. Firstly, the spectral filtering enables the multicolor operation of laser. Secondly, the convex–concave phase creates two opposite dispersion regimes for the generation of CS and DS. Finally, the group-delay compensation, together with the saturable absorption effect, synchronizes and overlaps the CS and DS, resulting in the unique HMSCs. It is demonstrated that the phase-managed fiber laser can deliver multicolor soliton compounds with distinct spectra and chirps, which provides an interesting platform to study the interaction of dissimilar solitons.

In summary, by introducing the convex–concave phase and spectral filtering, we demonstrate HMSCs comprised of CS and DS in an erbium-doped fiber laser. The CS and DS exhibit pairs of spectral sidebands obeying the same phase-matching principle. Especially, the spectral profile and pulse intensity of DS can be actively managed by tuning the amplitude of the concave phase. Simulations fully reproduce the experimental observations and indicate that the synchronization and overlap of two solitons rely on the group-delay compensation and saturable absorption effect. This work reveals a class of wavepackets, offers a simple testbed for exploring complex soliton interaction and may facilitate applications of terahertz wave generation and nonlinear spectroscopy.

Methods

Numerical simulations. The nonlinear Schrödinger equation in Eq. (3) models the propagation of pulse inside the cavity, and is solved by the predictor–corrector split-step Fourier technique^{29,50}:

$$\frac{\partial u}{\partial z} = -i\frac{\beta_2}{2}\frac{\partial^2 u}{\partial t^2} + i\gamma|u|^2u + \frac{(g-\alpha)}{2}u + \frac{g}{2\Omega_g^2}\frac{\partial^2 u}{\partial t^2}, \quad (3)$$

where u is the slowly varying envelope of the pulse, z and t represent the propagation distance and time, respectively. γ is the cubic refractive nonlinearity of the fiber and β_2 is the second-order dispersion coefficient. g , α , and Ω_g are the saturable gain, loss of the fiber and gain bandwidth, respectively. For the single-mode fiber, $g = 0$; and for the erbium-doped fiber, $g = g_0 \exp(-E_p/E_s)$, where g_0 , E_p , E_s are the small-signal gain coefficient, pulse energy, and the gain saturation energy, respectively. The saturable absorber has a transmittance $T = 0.46 - T_0/[1 + P_{(r)}/P_{sat}]$, where T_0 is the modulation depth, $P_{(r)}$ is the instantaneous pulse power, and P_{sat} is the saturable power. The spectral filter is modeled by a cosine function and has a transmittance $T_f(\omega) = [1 + 0.5\cos(d\omega)]/2$, where d is related to the filtering period.

The convex–concave phase is modeled by multiplying the electric field with the corresponding function in the frequency domain as $U_{out}(\omega) = U_{in}(\omega)\exp[i\varphi(\omega)]$, where $\varphi(\omega)$ is expressed as:

$$\varphi(\omega) = A(\omega - \omega_0)^2 + B(\omega - \omega_1)^2. \quad (4)$$

The first term on the right side of Eq. (4) is the convex phase, and the second term represents the concave phase. ω_0 and ω_1 denote the central angular frequencies of the convex and concave phases, respectively. The central angular frequency spacing between the convex and concave phases (i.e., $\omega_0 - \omega_1$) is the same as the period of the spectral filter.

The simulation parameter is set as follows to match the experiment: E_s are 340 pJ, 250 pJ, and 220 pJ, corresponding to the cases of Fig. 2a, Fig. 2b, and Fig. 2c, respectively. $T_0 = 0.08$, $P_{sat} = 8$ W. For the single-mode fiber, $g_0 = 0$, $\alpha = 4.6 \times 10^{-5} \text{ m}^{-1}$, $\beta_2 = -21.7 \text{ ps}^2 \text{ km}^{-1}$, $\gamma = 1.3 \text{ W}^{-1} \text{ km}^{-1}$. For the programmable pulse shaper, $\beta_2 = -120.3 \text{ ps}^2 \text{ km}^{-1}$, $\gamma = 0$. For the erbium-doped fiber, $g_0 = 0.7 \text{ dB m}^{-1}$, $\beta_2 = 21.3 \text{ ps}^2 \text{ km}^{-1}$, $\gamma = 3.9 \text{ W}^{-1} \text{ km}^{-1}$, $\Omega_g = 30 \text{ nm}$. For the spectral filter, $d = 1.53 \times 10^{-12} \text{ s}$. For the convex phase, A is -7.95 ps^2 during the whole simulation. For the concave phase, B is 7.95 ps^2 , 2.65 ps^2 , and 1.32 ps^2 , corresponding to the cases of Fig. 2a, Fig. 2b, and Fig. 2c, respectively.

Measurement system. The spectrum, pulse profile, signal-to-noise ratio, and pulse duration of HMSC are recorded by an optical spectrum analyzer (YOKOGAWA, AQ6370), a frequency-resolved optical gating (Femtoeasy, FS-600), a radio frequency analyzer (Agilent, E4440A) and an autocorrelator (Pulsecheck, USB-150), respectively. The time-stretch dispersive Fourier transform system comprises a 5-km dispersion compensation fiber with the dispersion of $-150 \text{ ps nm}^{-1} \text{ km}^{-1}$, a 4 GHz oscilloscope and a 5 GHz photodetector. Based on the above parameters, the overall spectral resolution of the system is calculated as 0.33 nm^{51} .

Reporting summary. Further information on research design is available in the Nature Portfolio Reporting Summary linked to this article.

Data availability

The data supporting the results of this paper are available from the corresponding author upon reasonable request.

Code availability

The simulation code is available upon reasonable written request, which excludes any commercial interest.

Received: 29 November 2022; Accepted: 19 July 2023;

Published online: 27 July 2023

References

- Wu, J., Keolian, R. & Rudnick, I. Observation of a nonpropagating hydrodynamic Soliton. *Phys. Rev. Lett.* **52**, 1421–1424 (1984).
- Kartashov, Y. V. & Konotop, V. V. Solitons in Bose-Einstein condensates with helicoidal spin-orbit coupling. *Phys. Rev. Lett.* **118**, 190401 (2017).
- Antipov, S., Nezhlin, M., Snezhkin, E. & Trubnikov, A. Rossby autosoliton and stationary model of the Jovian Great Red Spot. *Nature* **323**, 238–240 (1986).
- Davydov, A. S. Solitons and energy transfer along protein molecules. *J. Theor. Biol.* **66**, 379–387 (1977).
- Brida, D., Krauss, G., Sell, A. & Leitenstorfer, A. Ultrabroadband Er: fiber lasers. *Laser Photon. Rev.* **8**, 409–428 (2014).
- He, W., Pang, M., Menyuk, C. R. & St. J. Russell, P. Sub-100-fs 1.87 GHz mode-locked fiber laser using stretched-soliton effects. *Optica* **3**, 1366–1372 (2016).
- Oktem, B., Ülgüdür, C. & İlday, F. Ö. Soliton–similariton fibre laser. *Nat. Photonics* **4**, 307–311 (2010).
- Grelu, P. & Akhmediev, N. Dissipative solitons for mode-locked lasers. *Nat. Photonics* **6**, 84–92 (2012).
- Zou, J., Dong, C., Wang, H., Du, T. & Luo, Z. Towards visible-wavelength passively mode-locked lasers in all-fibre format. *Light Sci. Appl.* **9**, 61 (2020).
- Huang, S. et al. Tunable and switchable multi-wavelength dissipative soliton generation in a graphene oxide mode-locked Yb-doped fiber laser. *Opt. Express* **22**, 11417–11426 (2014).
- Wu, Z. et al. Dual-state dissipative solitons from an all-normal-dispersion erbium-doped fiber laser: continuous wavelength tuning and multi-wavelength emission. *Opt. Lett.* **40**, 2684–2687 (2015).
- Wei, Y., Li, B., Wei, X., Yu, Y. & Wong, K. K. Y. Ultrafast spectral dynamics of dual-color soliton intracavity collision in a mode-locked fiber laser. *Appl. Phys. Lett.* **112**, 081104 (2018).
- Mao, D., Liu, X., Han, D. & Lu, H. Compact all-fiber laser delivering conventional and dissipative solitons. *Opt. Lett.* **38**, 3190–3193 (2013).
- Wang, Y. et al. Coexistence of dissipative soliton and stretched pulse in dual-wavelength mode-locked Tm-doped fiber laser with strong third-order dispersion. *Opt. Express* **26**, 18190–18201 (2018).
- Jang, J. K. et al. Synchronization of coupled optical microresonators. *Nat. Photonics* **12**, 688–693 (2018).
- Majkić, A. et al. Terahertz source at 9.4 THz based on a dual-wavelength infrared laser and quasi-phase matching in organic crystals OH1. *Appl. Phys. Lett.* **105**, 141115 (2014).
- Kong, C. et al. High-contrast, fast chemical imaging by coherent Raman scattering using a self-synchronized two-colour fibre laser. *Light Sci. Appl.* **9**, 25 (2020).
- Shelton, R. K. et al. Subfemtosecond timing jitter between two independent, actively synchronized, mode-locked lasers. *Opt. Lett.* **27**, 312–314 (2002).
- Schibli, T. R. et al. Attosecond active synchronization of passively mode-locked lasers by balanced cross correlation. *Opt. Lett.* **28**, 947–949 (2003).
- Zeng, J. et al. Passively synchronized dual-color mode-locked fiber lasers based on nonlinear amplifying loop mirrors. *Opt. Lett.* **44**, 5061–5064 (2019).

21. Zhang, H. et al. Morphology-controllable ultrafast fiber lasers based on intracavity manipulation of transverse modes. *Phys. Rev. Appl.* **16**, 034045 (2021).
22. Hu, G. et al. Asynchronous and synchronous dual-wavelength pulse generation in a passively mode-locked fiber laser with a mode-locker. *Opt. Lett.* **42**, 4942–4945 (2017).
23. Wang, Z. et al. High-power synchronous multi-wavelength solitons from a multimode mode-locked fiber laser system. *Opt. Lett.* **46**, 118–121 (2021).
24. Babin, S. A. et al. Multicolour nonlinearly bound chirped dissipative solitons. *Nat. Commun.* **5**, 4653 (2014).
25. Iegorov, R., Teamir, T., Makey, G. & Ilday, F. Ö. Direct control of mode-locking states of a fiber laser. *Optica* **3**, 1312–1315 (2016).
26. Melchert, O. et al. Soliton molecules with two frequencies. *Phys. Rev. Lett.* **123**, 243905 (2019).
27. Liu, S., Cui, Y., Karimi, E. & Malomed, B. A. On-demand harnessing of photonic soliton molecules. *Optica* **9**, 240 (2022).
28. Runge, A. F. J., Hudson, D. D., Tam, K. K. K., Sterke, C. M. D. & Blanco-Redondo, A. The pure-quartic soliton laser. *Nat. Photonics* **14**, 492–497 (2020).
29. Mao, D. et al. Synchronized multi-wavelength soliton fiber laser via intracavity group delay modulation. *Nat. Commun.* **12**, 6712 (2021).
30. Lourdesamy, J. P. et al. Spectrally periodic pulses for enhancement of optical nonlinear effects. *Nat. Phys.* **18**, 59–66 (2022).
31. Zhang, S. et al. Dark-bright soliton bound states in a microresonator. *Phys. Rev. Lett.* **128**, 033901 (2022).
32. Zhang, S., Silver, J. M., Bi, T. & Del'Haye, P. Spectral extension and synchronization of microcombs in a single microresonator. *Nat. Commun.* **11**, 6384 (2020).
33. Xiao, L., Wang, T., Ma, W., Zhu, H. & Zhao, R. Switching and coexistence of stretched pulse and dissipative soliton in a hybrid mode-locked fiber laser. *Opt. Commun.* **522**, 128649 (2022).
34. Agrawal, G. P. *Nonlinear Fiber Optics* (Academic Press, New York, 2007).
35. Kelly, S. M. J. Characteristic sideband instability of periodically amplified average soliton. *Electron. Lett.* **8**, 806–807 (1992).
36. Chong, A., Renninger, W. H. & Wise, F. W. Properties of normal-dispersion femtosecond fiber lasers. *J. Opt. Soc. Am. B* **25**, 140–148 (2008).
37. Wise, F. W., Chong, A. & Renninger, W. H. High-energy femtosecond fiber lasers based on pulse propagation at normal dispersion. *Laser Photon. Rev.* **2**, 58–73 (2008).
38. Wright, L. G. et al. Mechanisms of spatiotemporal mode-locking. *Nat. Phys.* **16**, 565–570 (2020).
39. Herink, G., Jalali, B., Ropers, C. & Solli, D. R. Resolving the build-up of femtosecond mode-locking with single-shot spectroscopy at 90 MHz frame rate. *Nat. Photonics* **10**, 321–326 (2016).
40. Peng, J., Boscolo, S., Zhao, Z. & Zeng, H. Breathing dissipative solitons in mode-locked fiber lasers. *Sci. Adv.* **5**, eaax1110 (2019).
41. Liu, M. et al. Visualizing the “Invisible” soliton pulsation in an ultrafast Laser. *Laser Photon. Rev.* **14**, 1900317 (2020).
42. Kudelin, I., Sugavanam, S. & Chernysheva, M. Pulse-onset dynamics in a bidirectional mode-locked fibre laser via instabilities. *Commun. Phys.* **3**, 202 (2020).
43. Peng, J. et al. Real-time observation of dissipative soliton formation in nonlinear polarization rotation mode-locked fibre lasers. *Commun. Phys.* **1**, 20 (2018).
44. Liu, X. & Cui, Y. Revealing the behavior of soliton buildup in a mode-locked laser. *Adv. Photonics* **1**, 016003 (2019).
45. Nelson, L. E., Jones, D. J., Tamura, K., Haus, H. A. & Ippen, E. P. Ultrashort-pulse fiber ring lasers. *Appl. Phys. B* **65**, 277–294 (1997).
46. Jones, D. J., Chen, Y., Haus, H. A. & Ippen, E. P. Resonant sideband generation in stretched-pulse fiber lasers. *Opt. Lett.* **23**, 1535–1537 (1998).
47. Dennis, M. L. & Duling Iii, I. N. Third-order dispersion in femtosecond fiber lasers. *Opt. Lett.* **19**, 1750–1752 (1994).
48. Du, Y., Shu, X., Han, M. & Cheng, P. Numerical investigation of the resonant radiation from dissipative soliton fiber lasers at normal dispersion. *J. Opt. Soc. Am. B* **36**, 1233–1240 (2019).
49. Chong, A., Renninger, W. H. & Wise, F. W. All-normal-dispersion femtosecond fiber laser with pulse energy above 20 nJ. *Opt. Lett.* **32**, 2408–2410 (2007).
50. Bednyakova, A. & Turitsyn, S. K. Adiabatic soliton laser. *Phys. Rev. Lett.* **114**, 113901 (2015).
51. Goda, K. & Jalali, B. Dispersive Fourier transformation for fast continuous single-shot measurements. *Nat. Photonics* **7**, 102–112 (2013).

Acknowledgements

This work was supported by the National Key R&D Program of China (2017YFA0303800), the National Natural Science Foundation of China (11874300, 61805277, 62105264), the Fundamental Research Funds for the Central Universities (3102019JC008), and the Natural Science Foundation of Shaanxi Province (2021JC-09, 2019JQ-447).

Author contributions

H.Z. performed the experiments, carried out the numerical simulations and wrote the manuscript. D.M. designed the experiments, carried out the theoretical analysis and revised the manuscript. Y.D. and C.Z. plotted the figures and discussed the results. Z.S. and J.Z. contributed to the interpretation of the results and revising of the manuscript.

Competing interests

The authors declare no competing interests.

Additional information


Supplementary information The online version contains supplementary material available at <https://doi.org/10.1038/s42005-023-01313-x>.

Correspondence and requests for materials should be addressed to Dong Mao.

Peer review information *Communications Physics* thanks Xingliang Li and the other, anonymous, reviewer(s) for their contribution to the peer review of this work. A peer review file is available.

Reprints and permission information is available at <http://www.nature.com/reprints>

Publisher's note Springer Nature remains neutral with regard to jurisdictional claims in published maps and institutional affiliations.

 **Open Access** This article is licensed under a Creative Commons Attribution 4.0 International License, which permits use, sharing, adaptation, distribution and reproduction in any medium or format, as long as you give appropriate credit to the original author(s) and the source, provide a link to the Creative Commons licence, and indicate if changes were made. The images or other third party material in this article are included in the article's Creative Commons licence, unless indicated otherwise in a credit line to the material. If material is not included in the article's Creative Commons licence and your intended use is not permitted by statutory regulation or exceeds the permitted use, you will need to obtain permission directly from the copyright holder. To view a copy of this licence, visit <http://creativecommons.org/licenses/by/4.0/>.

© The Author(s) 2023